Near Field Source Investigation in Shrouded Propellers

Near-Field Pressure Investigation in Shrouded Propellers

Shane Sha*, Sergi Palleja-Cabre†, Paruchuri Chaitanya‡, and Phillip Joseph§
Institute of Sound and Vibration Research, University of Southampton, Southampton, SO17 1BJ, United Kingdom

Francesco Avallone¶
Department of Mechanical and Aerospace Engineering, Politecnico di Torino, Corso Duca degli Abruzzi, 24 - 10129 Turin

This paper investigates the near-field pressure of a shrouded propeller with particular emphasis on the physical nature of the in-duct pressure field. While previous studies on shrouded propellers generally either treated the source as an idealised acoustic source, or focused on mean flow effects, blade loading, wake dynamics, and far-field noise generation, limited attention has been paid to the measured or computed in-duct pressure signals. To address this issue, a combined experimental and numerical study is carried out using in-duct microphone measurements and lattice Boltzmann method (LBM) simulations. The analysis focuses on the axial and azimuthal pressure distributions at the blade passing frequencies (BPFs). The in-duct axial decay is shown to be well described by a potential field like exponential scaling, in contrast to the slower acoustic decay observed outside the duct. Modal decomposition is then applied on the in-duct pressures field at three axial planes upstream of the propeller plane to filter out the acoustic pressure components. The results indicate that the total in-duct pressure is dominated by the hydrodynamic contribution, providing new physical insight into the composition of shrouded propeller in-duct pressure and highlighting the importance of distinguishing acoustic and non-acoustic contributions when interpreting near-field measurements. Beyond investigating the in-duct pressure field, a proposed modal filtering procedure provides a practical means of extracting the acoustic modal content generated by the propeller, which can subsequently be used as a representative source input for analytical ducted propeller radiation models.

I. Introduction

A. Previous work

In recent years, numerous studies have investigated the sound field produced by shrouded propellers, driven by the increasing applications of ducted propulsion systems. One key aspect of this problem is the acoustic propagation and radiation in such 'short' ducts. Previous investigations of this problem [1–4] have assumed an idealised monopole or dipole source, and the main objective is to examine how the pressure propagates within the duct and radiates to the far-field. Such studies have provided important physical insight into the modal propagation and far-field directivity of 'short' ducts and the importance of the cut-off modes in this problem. Much of this literature has focused on infinite or semi-infinite duct configurations, with particular emphasis on the cut-off modes [3, 5], while more recent work has extended the analysis to finite-length ducts [2, 4]. These studies allow the propagation problem to be isolated and offer a valuable reference framework for understanding duct acoustic radiation. However, in practical shrouded propeller systems, the source characteristics themselves are a key aspect, including the unsteady aerodynamic loading on the blades and the flow structures generated by the propeller, which are naturally not included in the simple point source models used previously.

Pereira et al. [6] used wall-flush microphone measurements to perform modal identification of the in-duct pressure field in a small-scale ducted fan. Their objective was to decompose the measured tonal pressure into duct acoustic modes and identify the dominant modal content at the first three blade passing frequencies (BPFs), where the strongest modes were successfully extracted. They also showed that this approach becomes much more difficult in the broadband

*PhD student, ISVR, University of Southampton
†Senior Research Fellow, Institute of Sound & Vibration Research, University of Southampton
‡Associate Professor, Institute of Sound & Vibration Research, University of Southampton
§Professor, Institute of Sound & Vibration Research, University of Southampton
¶Professor, Politecnico di Torino

regime, because the in-duct wall pressure measurements are strongly contaminated by turbulent boundary layer (TBL) related hydrodynamic fluctuations, which must be suppressed before reliable modal identification can be achieved. However, this methodology does not explicitly decouple the hydrodynamic and acoustic contributions before the modal analysis, and therefore does not directly reveal the physical composition of the total in-duct pressure field or establish to what extent the measured tonal pressure is purely acoustic in nature.

Go et al. [7] conducted experimental and numerical investigations of the sound field produced by a shrouded propeller. They found that the pressure decays exponentially in the axial direction, while at the propeller plane it reaches minima at various BPF harmonics. However, their focus was on comparing the different noise sources for shrouded and unshrouded propellers.

Most recently, Palleja Cabre et al. [8, 9] conducted experiments on a shrouded propeller and compared the measured in-duct axial pressure decays with the acoustic pressures calculated by the analytical model. They found that the decays inside the duct cannot be captured by the analytical model, suggesting that the decays are not purely acoustic decays of the evanescent modes and the near-field hydrodynamic pressure plays a significant role in the measured in-duct pressures.

Recent studies on shrouded propellers have also increasingly considered operating conditions with non-zero mean flow rather than hovering alone. In particular, attention has been given to how the presence of the shroud modifies the mean flow field and thereby influences the resulting aeroacoustic radiation. For example, Go et al. [10–12] developed a series of theoretical and experimental studies on the turbulent inflow noise of shrouded propellers, in which the propeller induced mean flow and the shroud alter the distortion of the ingested turbulence, leading to unsteady blade loading and subsequent far-field sound radiation, while the shroud also affects the acoustic scattering of the radiated sound. Similarly, Cantos et al. [13] investigated a ducted propeller under axial inflow and focused on the coupled changes in aerodynamic performance, wake flow structure, and radiated noise. Their measurements showed that axial flow affects not only the mean loading of the propeller and duct, but also the wake turbulent structures and both tonal and broadband far-field noise characteristics.

B. Scope and objectives

Although a considerable body of work exists on shrouded propellers, to the authors' knowledge, limited attention has been paid to the physical composition of the in-duct near-field pressure of shrouded propellers, particularly to the distinction between acoustic and hydrodynamic contributions. In particular, existing studies have seldom examined to what extent the measured or computed in-duct pressure should be interpreted as a purely acoustic field, or whether it also contains a substantial hydrodynamic contribution. This distinction is important because, without first identifying the non-acoustic component of the total pressure field, it is difficult to determine how the acoustic pressure generated by the propeller propagates and decays within the duct and subsequently radiates to the far field. This paper therefore focuses on the physical interpretation of the in-duct pressure field of a shrouded propeller. Specifically, the objectives of the paper are:

(a) Analyse the axial decay of the total in-duct pressure obtained from both LBM simulations and experiments at different BPFs, and how this decay outside of the duct as it approaches the acoustic far-field; and

(b) Apply a modal decomposition to the pressure field from three planes at different axial locations upstream of the propeller plane in order to filter out the acoustic pressure component.

II. Methodology

A. Experimental setup

The experiments were carried out on the modular shroud rig shown in Fig. 1 and described in [14]. The rotor is powered by a U7-V2.0 KV420 Brushless T-motor mounted on a MINI45 ATI 6-axis loadcell. The propeller, the motor and the loadcell are held on the axis of the shroud by a vertical rod located downstream of the propeller plane. The electronic speed controller used in conjunction with the motor is a Master Mezon 135 opto unit. To measure the rotational speed of the propeller (rotations per minute, RPM) an ICP Laser Tachometer sensor is used. A 2-bladed MEJZLIK propeller with a diameter of 16 inches was used in the current investigation.

The modular shroud was designed to allow for different lengths and install acoustic treatments such as liners. In this paper, the experimental data used was measured with a duct 250 mm long and with a 'lip' intake. The acoustic performance of different intake shapes are out of the scope of this current paper and the 'lip' intake is a more

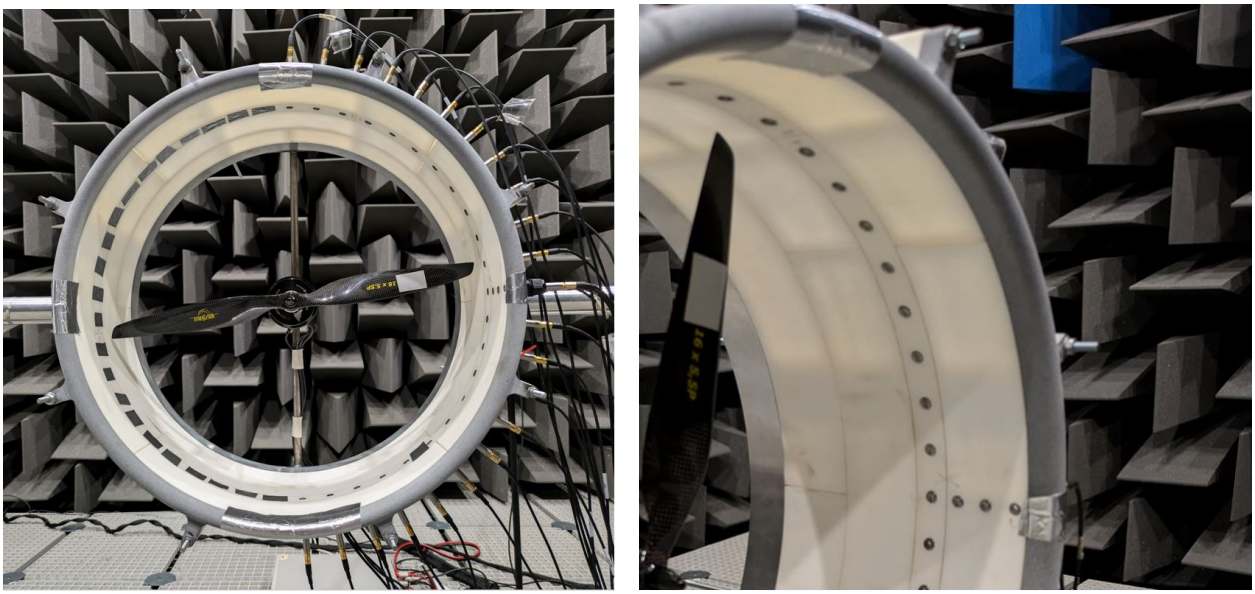

(a) Front view **(b) Detail view**

Fig. 1 Shrouded propeller rig of the in-duct instrumentation.

representative model for a real aerodynamic intake geometry [8], which was therefore used in the experiment. The propeller is located at fixed axial distances from the duct inlet z_0 =150 mm. A constant propeller thrust of T=10 N was applied and the corresponding RPM was measured as RPM_{duct} = 4582.

The experiments were carried out at the Institute of Sound and Vibration Research's anechoic chamber, of dimensions 6.7 m × 6.7 m × 4.9 m. The chamber's walls are acoustically treated with open-cell polyurethane wedges whose cut-off frequency is 70 Hz. In-duct and far-field noise measurements were obtained by using quarter-inch GRAS 40PL-10 CCP microphones. Far-field noise measurements were obtained by using 3 microphones positioned at a radius of 2.5 m from the propeller rig at angles relative to the propeller axis of $\phi = 0°, 45°$and 90°. In-duct noise measurements were obtained by installing instrumentation modules with in-duct microphone arrays. In duct noise measurements were taken by using 25 microphones: 4 microphones located in the axial module and 22 microphones on the circumferential module, one microphone was used for both the axial and azimuthal measurements. The axial microphones were located at 32 mm, 50 mm, 68 mm and 85 mm respectively upstream of the propeller plane, while the azimuthal microphones were located at the same axial location of 85 mm upstream of the propeller plane, with azimuthal angles ranging from −90° to 90° with respect to the horizontal plane. Measurements were carried out for a duration of 10 s at a sampling frequency of 40 kHz.

B. CFD simulations

The LB method is used to compute the flow field because it was shown to be accurate and efficient in the presence of complex flow problems [15]. The commercial software 3DS Simulia PowerFLOW 6-2025 is used. The software solves the discrete LB equation for a finite number of directions. For a detailed description of the method, the reader can refer to Succi [16] and Shan et al. [17], while to Chen and Doolen [18] for a review. The LB method determines the macroscopic flow variables starting from the mesoscopic kinetic equation, i.e. the LB equation. The discretization used for this particular application consists of 19 discrete velocities in three dimensions (D3Q19), involving a third-order truncation of the Chapman-Enskog expansion [19]. The distribution of particles is solved by means of the LB equation on a Cartesian mesh, known as a lattice. An explicit time integration and a collision model are used. For the collision term, the formulation based on a unique Galilean invariant [20] is used. The equilibrium distribution of Maxwell-Boltzmann is adopted [19].

A very large eddy simulation (VLES) model is implemented to take into account the effect of the sub-grid unresolved scales of turbulence. Following Yakhot and Orszag [21], a two-equation $k - \epsilon$ Renormalization Group is used to compute a turbulent relaxation time that is added to the viscous relaxation time. To reduce the computational cost, a

pressure-gradient-extended wall model is used to approximate the no-slip boundary condition on solid walls [22, 23]. The model is based on the extension of the generalized law-of-the-wall model [24] to take into account the effect of pressure gradient. These equations are iteratively solved from the first cell close to the wall in order to specify the boundary conditions of the turbulence model. For this purpose, a slip algorithm [18], obtained as generalization of a bounce-back and specular reflection process, is used.

The simulation domain is a box of length equal to 10 m. The rotor plane is placed downstream of the inlet. Free-stream inlet boundary conditions upstream while pressure outlet boundary conditions are applied on all the other sides of the domain. Slip boundary conditions are applied at the other walls. A total of 13 mesh refinement regions, named VR, with a resolution factor of 2, are employed. The region with the highest resolution is in the tip gap region and close to the blade surface, where the voxel size is $\approx 3.9 \times 10^{-4}$ m, corresponding to 1800 voxels per duct chord. This guarantees a sufficient number of voxels in the tip gap region [15]. An acoustic sponge region is used to damp unwanted reflections of the acoustic waves at the boundaries of the computational domain. This is achieved by increasing the viscosity by a factor of 100 starting from a radius of 2.5 m away from the centre of the duct. A convergence study was conducted before any simulation which is not shown here.

Simulations were run for 14 rotor revolutions after the initial transient. Data are saved at a frequency of 40 kHz.

III. Results

This section presents the results from both the LBM simulations and the experiments. A schematic diagram showing the shrouded propeller and microphone locations is shown in Fig. 2. The duct has a length L of 250 mm including the 'lip' intake, among which 150 mm is upstream of the propeller plane, while the remaining 100 mm is downstream of it. The radius of the duct is $a = 0.205$ m.

As mentioned in the last section, there are 25 in-duct microphones: 4 axial microphones and 22 azimuthal microphones with angles from $-90°$ to $90°$, for the experiments. However, for the LBM model, while the ducted propeller configuration remains the same, the pressure can be obtained at all azimuthal angles and at different axial locations, both inside and outside the duct.

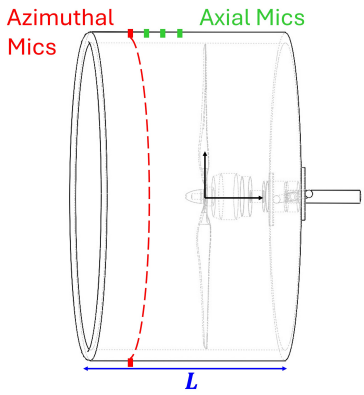

Fig. 2 Shrouded propeller and microphones setup

A. Time-domain pressure signals

The time-domain pressure signals at selected axial locations along the duct wall are first presented. The four axial microphone locations used in the experiments are included to validate the LBM model. The results are shown in Fig. 3.

The comparison of the measured data and numerical results in Fig. 3(c) to Fig.3(f) show a close agreement at all axial locations, thereby validating the numerical model. It can be observed that the pressure signals inside the duct present high-amplitude periodic fluctuations. The pressure values inside the duct vary between ± 100 Pa, which suggests that the pressure field is dominated by hydrodynamic pressure. However, the pressures outside the duct, shown in Fig. 3(a) and Fig. 3(b), are qualitatively very different from what those inside the duct, in which there are no periodic pressure drops and also the pressure values are much smaller in magnitude, which suggests that these pressure fluctuations are primarily acoustic.

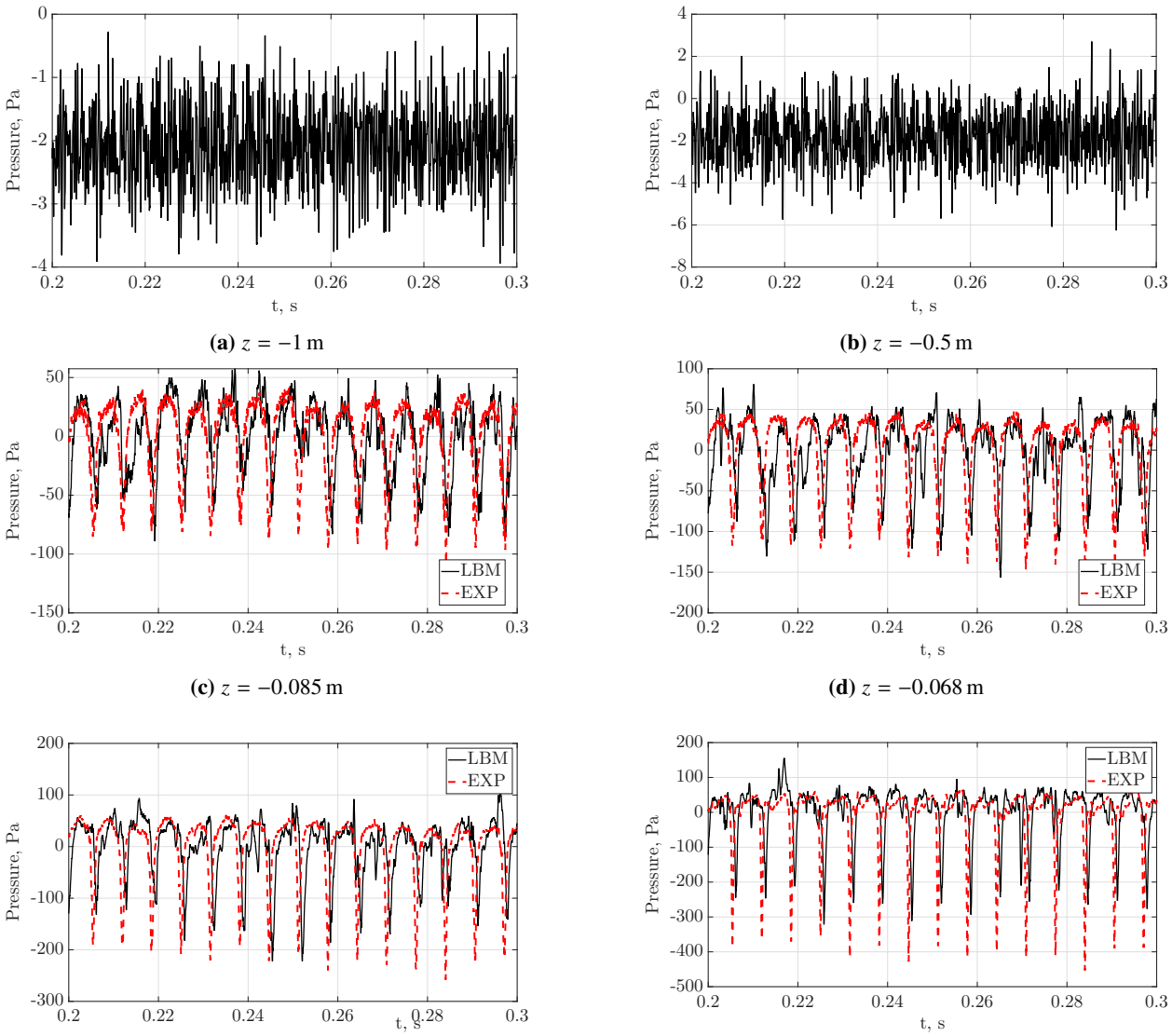

(a) $z = -1$ m

(b) $z = -0.5$ m

(c) $z = -0.085$ m

(d) $z = -0.068$ m

(e) $z = -0.05$ m

(f) $z = -0.032$ m

Fig. 3 Time histories of pressure at different axial locations.

B. In-duct pressure spectrum

The in-duct pressure spectra obtained from the LBM simulations is compared with the experimental measurements at different axial locations in Fig. 4. Overall, an excellent agreement is observed between the numerical and experimental spectra at all in-duct axial locations. In particular, the tonal levels at the first few BPF harmonics are captured very well by the LBM model, which further increases confidence in the numerical data used for the subsequent in-duct pressure analysis.

Both the LBM and experimental results show that the tonal components are significantly stronger than the broadband contribution. This indicates that the in-duct pressure field is dominated by periodic blade passing events, most likely associated with the unsteady blade loading. The clear dominance of the tonal components justifies the subsequent focus on the first three BPF harmonics, for which the axial decay and modal content are examined in detail. It can also be observed that the relative levels of the tonal peaks vary with axial position. The higher BPF harmonics decrease more rapidly with increasing distance from the propeller plane. This behaviour is examined in more detail in the following section, where the axial pressure decay at the first three BPFs is analysed.

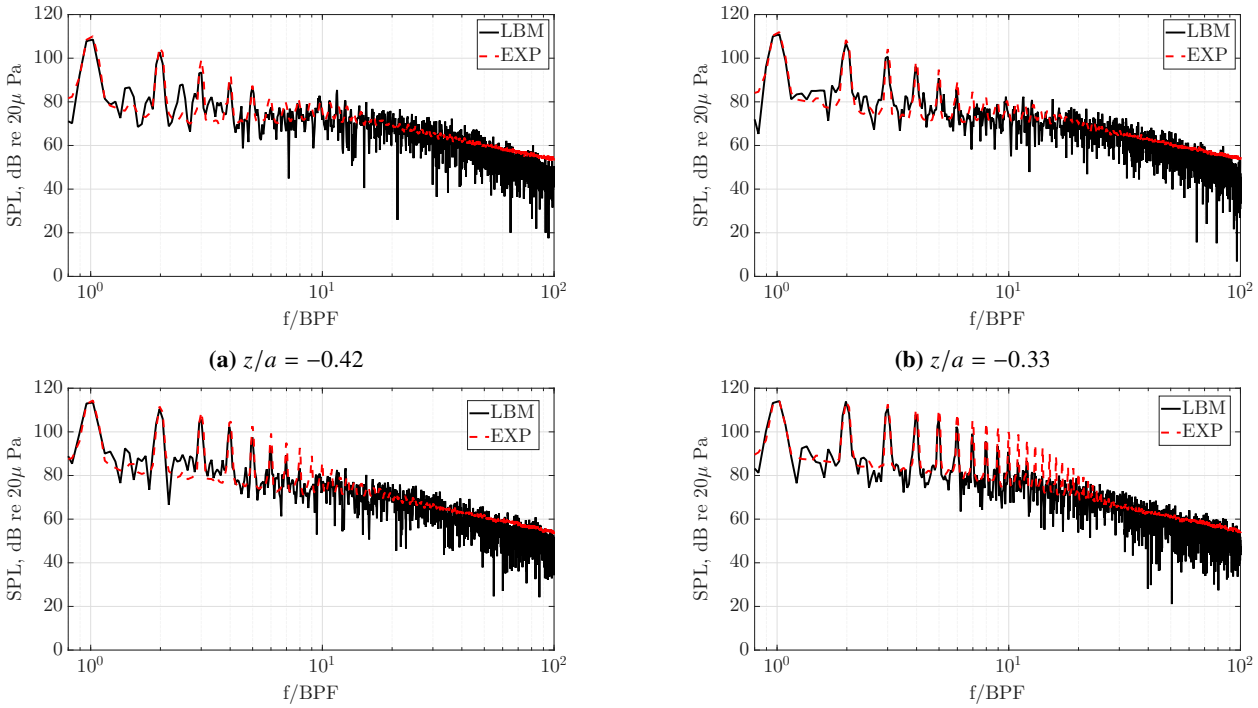

(a) $z/a = -0.42$ **(b)** $z/a = -0.33$

(c) $z/a = -0.24$ **(d)** $z/a = -0.16$

Fig. 4 In-duct pressure spectrum at different axial locations upstream of the propeller plane ($z_p/a = 0$).

C. Axial decay of the pressure field

As mentioned in the previous section, the in-duct wall pressure decreases in magnitude from the propeller plane towards the duct intake due to axial decay inside the duct. The axial decay of the pressure inside the duct obtained with the LBM simulations for the first three BPFs is shown in Fig. 5(a). The pressures measured by the four axial microphones in the experiments are also plotted for comparison.

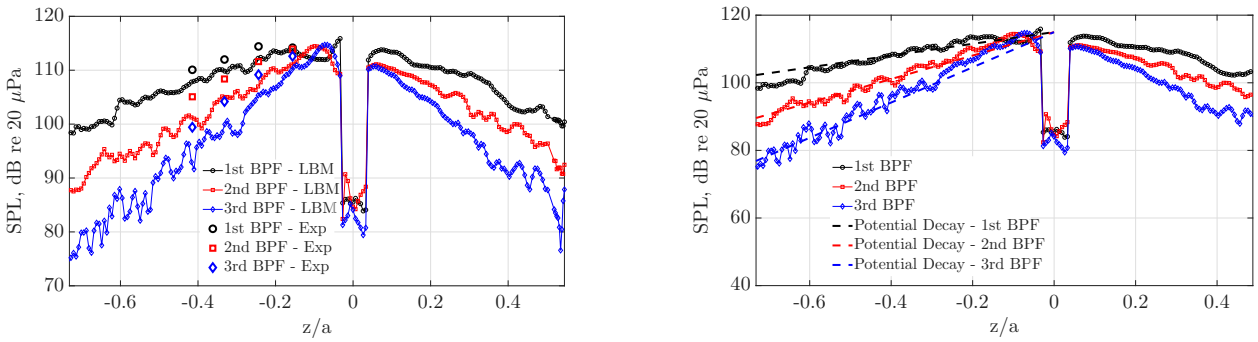

(a) LBM model vs experiments **(b) LBM model vs the potential field model**

Fig. 5 In-duct axial pressure decays for the first three BPFs.

The experimental results in Fig. 5(a) show similar decay rates to those predicted by the LBM model for all three BPFs, although the absolute pressure levels differ by approximately 1 to 4 dB. The decays are approximately exponential, and the decay rate varies with frequency, in which the decay rate is faster at higher frequencies. These behaviour was also observed in the decay of the bound potential field in the context of contra rotating open rotors (CRORs) by. Parry [25], who described the bound potential field in terms of harmonic components. The exponential decay term due to the axial distance to the propeller plane can be written as:

$$E_x = \exp\left[-\frac{2\pi\beta|n|\,|z|}{s\left(\sin^2\alpha+\beta^2\cos^2\alpha\right)}+\frac{i\,2\pi\left(1-\beta^2\right)nz\sin\alpha\cos\alpha}{s\left(\sin^2\alpha+\beta^2\cos^2\alpha\right)}\right] \quad , \tag{1}$$

where $|z|$ is the axial distance from the propeller plane, n is number of harmonics, α is the blade stagger angle, $s = 2\pi a/B$, is the distance between the blades (B is the number of blades), and $\beta = \sqrt{1-M^2}$ is the Mach number factor where M is the Mach number. Therefore, for a fixed configuration of the propeller and flow condition, the exponential decay term can be simplified into:

$$|E_x| \propto \exp\left(-\frac{B|n||z|}{a}\right) \quad . \tag{2}$$

The potential-field decay predicted by Eq. 2 is compared with the LBM in-duct pressure results for the first three BPFs in Fig. 5(b). The results show a close agreement, which suggests that the pressures inside the duct are dominated by the hydrodynamic effects and the decays can be described primarily by the decay of the propeller bound potential field.

The axial pressure decays from the propeller plane all the way to $z/a \approx -6$, which is around 1.2 m from the propeller plane, is shown in Fig. 6. Also shown in Fig. 6 is the decay of an axial acoustic dipole source, which is proportional to:

$$P_{\text{dipole}} \propto cos\theta e^{-jkr}\left(\frac{jk}{r}+\frac{1}{r^2}\right) \quad , \tag{3}$$

where k is the acoustic wavenumber which is related to the BPF and r is the distance from the source to the receiver.

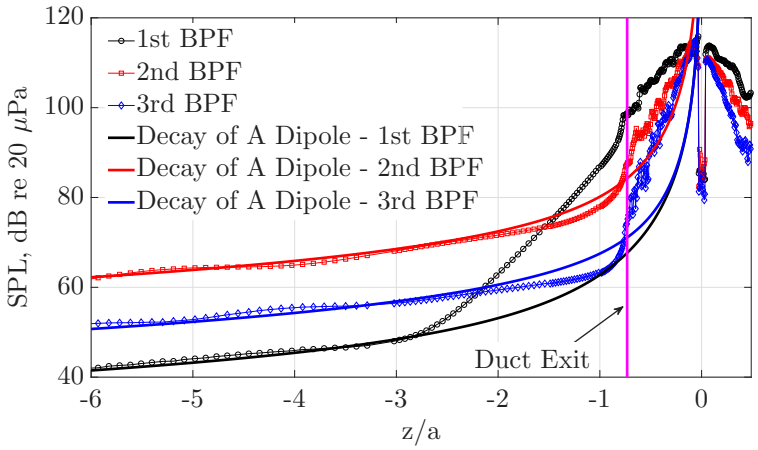

Fig. 6 Axial pressure decays from the propeller plane to the far-field from the LBM model and the analytical model for a dipole acoustic source at first three BPFs.

Apart from the first BPF, the axial decay rates at the other BPFs agree with those predicted by Eq. 3, specially for $z/a < -2$, that from around 0.41 m from the propeller plane. In contrast, the decay rate for the first BPF remains close to the potential field decay even after leaving the duct and collapses to the acoustic field decay only fpr $z/a < -3$, that is from around $z = 0.615$ m. This matches with the time domain signals shown in Fig. 3(a) and Fig. 3(b) that at these axial locations, the pressures become pure acoustic pressures.

The comparison between the potential field scaling and the acoustic decay model suggests that the total in-duct pressure contains a strong bound near-field component that is not described by a propagating duct acoustic model. However, this does not imply that the acoustic component is absent. Rather, it indicates that the acoustic contribution is masked by the larger non-acoustic near-field pressure. A modal decomposition is therefore required to isolate the acoustic pressure components.

D. Far-field pressure spectrum

The far-field pressure spectra at different polar observation angles are shown in Fig. 7 measured at a radial distance of approximately 2.5 m. At $\theta = 0°$ and $\theta = 45°$, the LBM model under predicts the pressure level at the first BPF. This is consistent with the axial pressure results shown in Fig. 6, where the first BPF level outside the duct is lower than those of the higher BPF harmonics in the LBM data. This is in contrast with the close agreement between the experiments and the simulations in the in-duct wall pressures and needs further investigation.

Despite these discrepancies in the absolute tonal levels, both the LBM and experimental results show that the far-field spectrum is still dominated by tonal components associated with the BPF harmonics. This is consistent with the in-duct pressure spectra discussed above, where the tonal components were also found to be significantly stronger than the broadband contribution.

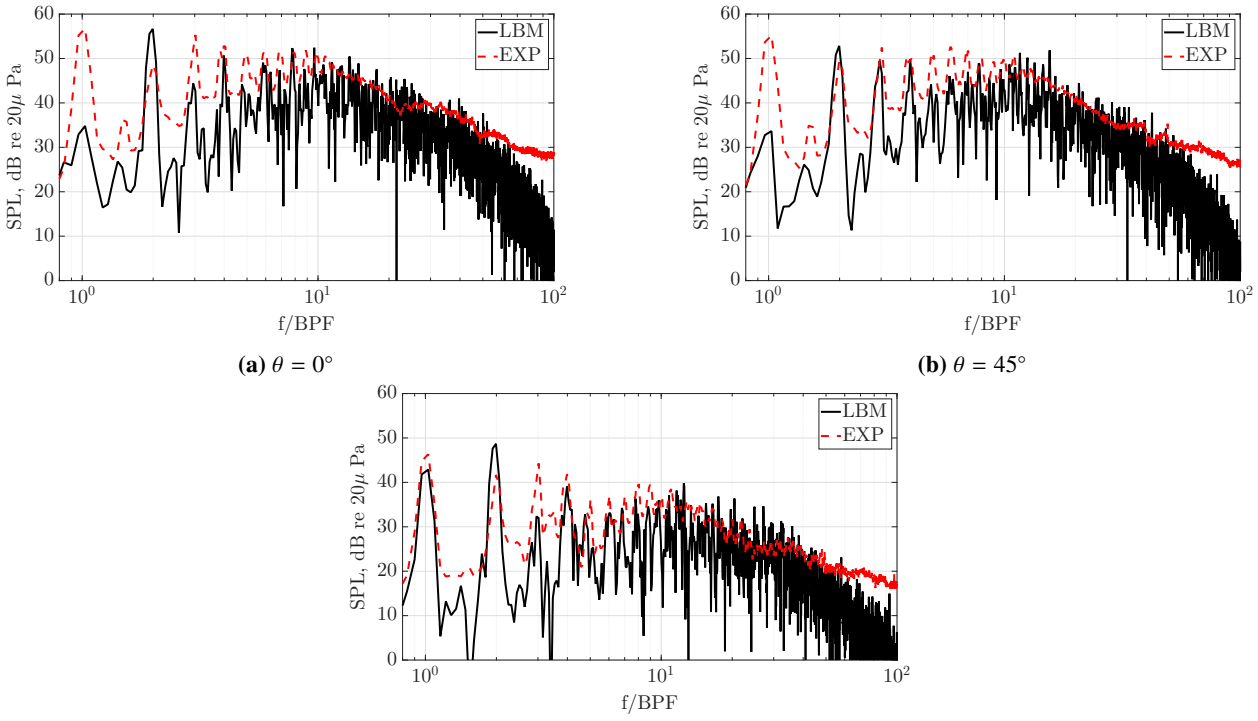

(a) $\theta = 0°$ **(b)** $\theta = 45°$

(c) $\theta = 90°$

Fig. 7 Far-field pressure spectrum at different polar angles.

E. Modal decomposition

The total pressure field obtained from the LBM model can be expressed as the sum of an acoustic pressure component, represented by a set of orthogonal duct modes $\Psi_{mn}(r, \theta)$, and a flow induced pressure component:

$$p(z, r, \theta) = \sum_{m,n} p_{mn}(z)\Psi_{mn}(r, \theta) + p_{flow} \quad . \tag{4}$$

The modes satisfy the orthogonality relation:

$$\langle \Psi_{mn}, \Psi_{pq} \rangle = N_{mn}\delta_{mp}\delta_{nq}, \tag{5}$$

where the inner product over the duct cross-section is defined as

$$\langle \Psi_{mn}, \Psi_{pq} \rangle = \int_0^{2\pi} \int_0^a \Psi_{mn}(r, \theta)\Psi^*_{pq}(r, \theta)\, r\, dr\, d\theta. \tag{6}$$

Therefore, multiplying the pressure expansion by Ψ^*_{mn} and integrating over the cross-section gives:

$$\int_0^{2\pi}\int_0^a p(z,r,\theta)\Psi^*_{mn}(r,\theta)\,r\,dr\,d\theta = \sum_{p,q} p_{pq}(z)\int_0^{2\pi}\int_0^a \Psi_{pq}(r,\theta)\Psi^*_{mn}(r,\theta)\,r\,dr\,d\theta. \tag{7}$$

Using the orthogonality relation, this becomes:

$$\int_0^{2\pi}\int_0^a p(z,r,\theta)\Psi^*_{mn}(r,\theta)\,r\,dr\,d\theta = p_{mn}(z)N_{mn}. \tag{8}$$

Hence, the modal coefficient at axial location z is:

$$p_{mn}(z) = \frac{\displaystyle\int_0^{2\pi}\int_0^a p(z,r,\theta)\Psi^*_{mn}(r,\theta)\,r\,dr\,d\theta}{\displaystyle\int_0^{2\pi}\int_0^a |\Psi_{mn}(r,\theta)|^2\,r\,dr\,d\theta}. \tag{9}$$

The mode shape function $\Psi_{mn}(r,\theta)$ is normalised and can be expressed as:

$$\Psi_{mn}(r,\theta) = \frac{J_m(\kappa_{mn}r)}{\sqrt{1-(m^2/\kappa_{mn}^2a^2)}J_m(\kappa_{mn}a)}e^{jm\theta} \quad , \tag{10}$$

where κ_{mn} are the eigen-solutions for the hard wall boundary conditions satisfying:

$$J'_m(\kappa_{mn}a) = 0 \quad . \tag{11}$$

From Eq. 10, it can be demonstrated that $\Psi_{mn}(r,\theta)$ satisfies:

$$\frac{1}{S}\int |\Psi_{mn}(r,\theta)|^2 dS = 1 \quad , \tag{12}$$

where S is the cross-sectional area of the duct and is calculated as $S = \pi a^2$. Therefore, N_{mn} can be calculated as:

$$N_{mn} = \int_0^{2\pi}\int_0^a |\Psi_{mn}(r,\theta)|^2\,r\,dr\,d\theta = S, \tag{13}$$

then:

$$p_{mn}(z) = \frac{1}{S}\int_0^{2\pi}\int_0^a p(z,r,\theta)\Psi^*_{mn}(r,\theta)\,r\,dr\,d\theta. \tag{14}$$

The axial wavenumber is given by the dispersive relation:

$$k^2_{z,mn} = k^2 - \kappa^2_{mn} \quad , \tag{15}$$

where $k = \omega/c_0$ is the acoustic wavenumber. The modal coefficient can then be written as a superposition of positive and negative going travelling waves:

$$p_{mn}(z) = a^+_{mn}e^{-jk_{z,mn}z} + a^-_{mn}e^{jk_{z,mn}z} \quad . \tag{16}$$

For a specific mode, the modal coefficients obtained at three axial planes z_1, z_2 and z_3 satisfy:

$$\begin{bmatrix} p_{mn}(z_1) \\ p_{mn}(z_2) \\ p_{mn}(z_3) \end{bmatrix} = \begin{bmatrix} e^{-jk_{z,mn}z_1} & e^{jk_{z,mn}z_1} \\ e^{-jk_{z,mn}z_2} & e^{jk_{z,mn}z_2} \\ e^{-jk_{z,mn}z_3} & e^{jk_{z,mn}z_3} \end{bmatrix} \begin{bmatrix} a^+_{mn} \\ a^-_{mn} \end{bmatrix} \quad . \tag{17}$$

This system can be solved with the inverse matrix:

$$\begin{bmatrix} a^+_{mn} \\ a^-_{mn} \end{bmatrix} = \mathbf{A}^\dagger \begin{bmatrix} p_{mn}(z_1) \\ p_{mn}(z_2) \\ p_{mn}(z_3) \end{bmatrix} \quad , \tag{18}$$

where

$$\mathbf{A} = \begin{bmatrix} e^{-jk_{z,mn}z_1} & e^{jk_{z,mn}z_1} \\ e^{-jk_{z,mn}z_2} & e^{jk_{z,mn}z_2} \\ e^{-jk_{z,mn}z_3} & e^{jk_{z,mn}z_3} \end{bmatrix} \quad , \tag{19}$$

and $\mathbf{A}^{\dagger}$ denotes the inverse matrix.

In practice, the pressure data from the LBM simulation are first interpolated onto a structured polar grid (r_i, θ_j). The modal coefficient is then approximated numerically as:

$$p_{mn}(z) \approx \frac{1}{S} \sum_{i=1}^{N_r} \sum_{j=1}^{N_\theta} p(z, r_i, \theta_j) \Psi^*_{mn}(r_i, \theta_j) r_i \, \Delta r \, \Delta\theta. \tag{20}$$

Therefore, the radial and azimuthal spacings, Δr and $\Delta\theta$, are required to evaluate the modal projection integral. The reconstructed acoustic pressure can therefore be written as:

$$p_{rec}(z, r, \theta) = \sum_{m,n} p_{mn}(z) \Psi_{mn}(r, \theta). \tag{21}$$

When a one way upstream reconstruction is required, the upstream going cut-on contribution and the upstream decaying cut-off contribution are retained:

$$p^{\mathrm{up}}_{\mathrm{rec}}(z, r, \theta) = \sum_{m,n} a^{-}_{mn} e^{jk_{z,mn}z} \Psi_{mn}(r, \theta) \quad , \tag{22}$$

In this way, the modal projection acts as an acoustic filter: only the pressure components that satisfy the assumed acoustic modal formulation are retained in p_{ac}. The remaining components, including hydrodynamic pressure fluctuations, are excluded from the reconstruction. This modal decomposition method therefore relies on the assumption that:

$$\frac{1}{S} \int_S p_{flow} \Psi dS \approx 0 \quad . \tag{23}$$

The in-duct and downstream pressure levels obtained from the LBM simulations are compared with the acoustic pressure reconstructed using the modal decomposition in Fig. 8. The reconstructed results are shown both for pressure which includes cut-off modes and for the propagating cut-on modes only. It can be observed that for the first and second BPFs, the reconstructed acoustic pressure including cut-off modes approaches the reconstruction with onlt the cut-on modes by the duct exit. This indicates that the evanescent cut-off modal components have largely decayed before the pressure reaches the exit plane. In contrast, for the third BPF, a noticeable difference remains between the two solutions near the duct exit, suggesting that some cut-off modal content is still present at this location. This behaviour is consistent with the cut-off modes decay length discussed in [4], but it is unexpected that the reconstructed solution leads to a higher magnitude than the simulated pressures, which could possibly indicate that the filtering is not capable of completely removing the hydrodynamic contributions in the pressure field.

Overall, the results demonstrate that the modal decomposition provides a useful means of reconstructing the in-duct acoustic pressure generated by the shrouded propeller. More importantly, the comparison with the total LBM pressure signals confirms that the pressure measured inside the duct should not be interpreted as purely acoustic. The total in-duct pressure contains a substantial non-acoustic near-field contribution in addition to the acoustic modal component.

Fig. 9 and Fig. 10 show the modal amplitudes $|p_{mn}|$ reconstructed at the propeller plane ($z = 0\,\mathrm{m}$) and duct exit ($z = -0.15\,\mathrm{m}$), respectively. At the propeller plane, cut-off modes are present for all BPFs, the amplitudes of the cut-off modes are much higher than those of the cut-on modes, especially for strongly cut-off modes, which may be because the assumption in Eq. 23 is not fully satisfied and some flow induced pressure content is also projected onto these modes.

However, when at the duct exit, for the first and second BPFs, the modal content at the duct exit is dominated by the cut-on modes, indicating that the cut-off modal components have largely decayed before reaching the exit plane. In contrast, at the third BPF, the cut-off modes $(m, n) = (-1, 1)$ and $(1, 1)$ still exhibit appreciable amplitudes at the duct exit. The modal amplitudes at the duct exit are particularly important because they represent the acoustic modal content that is available to propagate out of the duct and contribute to the radiated sound field. Unlike the total in-duct pressure, which contains both acoustic and non-acoustic near-field contributions, the reconstructed modal amplitudes provide a source description that is consistent with the duct acoustic formulation. This allows the modal decomposition to be

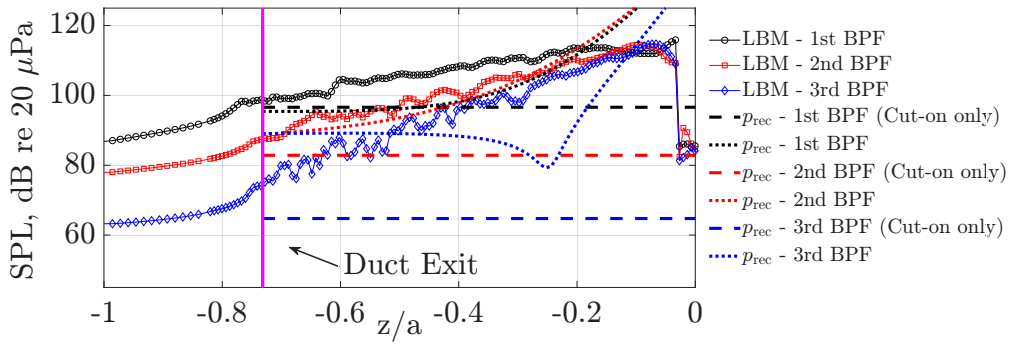

Fig. 8 Total pressure calculated by the LBM model vs reconstructed acoustic pressure through modal decompositions.

interpreted not only as a filtering procedure, but also as a means of obtaining a more representative acoustic source description for subsequent duct radiation predictions. This has practical implications for acoustic source modelling of shrouded propellers. Analytical duct radiation models commonly require the acoustic source to be prescribed in terms of idealised monopole, dipole, or modal source distributions. However, the present results show that the total in-duct pressure field is strongly influenced by non-acoustic near-field contributions and therefore cannot be used directly as an acoustic source measure. By extracting the part of the pressure field that is consistent with the duct acoustic modes, the present method provides a more representative modal source distribution for the propeller. The resulting modal amplitudes may then be used as input to analytical duct radiation models to predict acoustic propagation and radiation.

IV. Conclusions

This paper has examined the physical nature of the near-field pressure of a shrouded propeller, with particular focus on the in-duct pressure field obtained from experiments and LBM simulations. The results show that the numerical predictions reproduce the main experimental trends at the axial microphone locations, providing confidence in the use of the LBM data for further interpretation of the in-duct pressure field.

The time domain analysis revealed a clear distinction between the pressures inside and outside the duct. Inside the duct, except at the propeller plane, the pressure signals exhibit a pronounced periodic structure and relatively large amplitudes, whereas outside the duct, the fluctuations are much weaker and no longer display the same periodic behaviour. This already suggests that the in-duct pressure field is dominated by the hydrodynamic component.

The axial pressure results showed that, for the first three BPFs, the in-duct pressure decays approximately exponentially with axial distance from the propeller plane, with faster decay at higher harmonics. The measured and computed trends were found to be consistent, and the in-duct decay was in close agreement with the analytical solution of the decay of the potential field for CROR. This indicates that the total pressure inside the duct is not adequately described as a purely propagating acoustic field. Outside the duct, the pressure decay transitions towards that of an axial point dipole source as the potential field becomes weaker and the acoustic component dominates. The higher harmonics approach this regime earlier than the first BPF due to a faster decay of the hydrodynamic potential field.

The modal decomposition further shows that the acoustic component of the in-duct pressure can be separated from the total pressure field by projecting the LBM pressure signals onto an orthogonal duct mode basis. This provides a practical acoustic filtering procedure and confirms that the large pressure amplitudes observed inside the duct are not necessarily representative of the acoustic source. The extracted modal amplitudes provide a representative description of the acoustic source content generated by the propeller. These amplitudes can be used as input to analytical duct radiation models, replacing idealised source assumptions with modal source strengths obtained directly from the simulated propeller field, and allowing models such as that in [4] to be validated against numerical and experimental data.

However, the present modal decomposition also reveals some limitations. The reconstructed modal amplitudes p_{mn} at the propeller plane, $z_p = 0$, do not fully follow the expected trend, since some strongly cut-off modes exhibit relatively large amplitudes. This indicates that the assumption made in Eq. 23 may not be fully adequate close to the propeller plane, in which part of the hydrodynamic or potential-field pressure may still be projected onto the acoustic duct-mode basis. In addition, the reconstructed in-duct acoustic pressure for the third BPF is less satisfactory than for the lower harmonics, as shown in Fig. 8, suggesting that a more refined modal filtering strategy should be explored in future work.

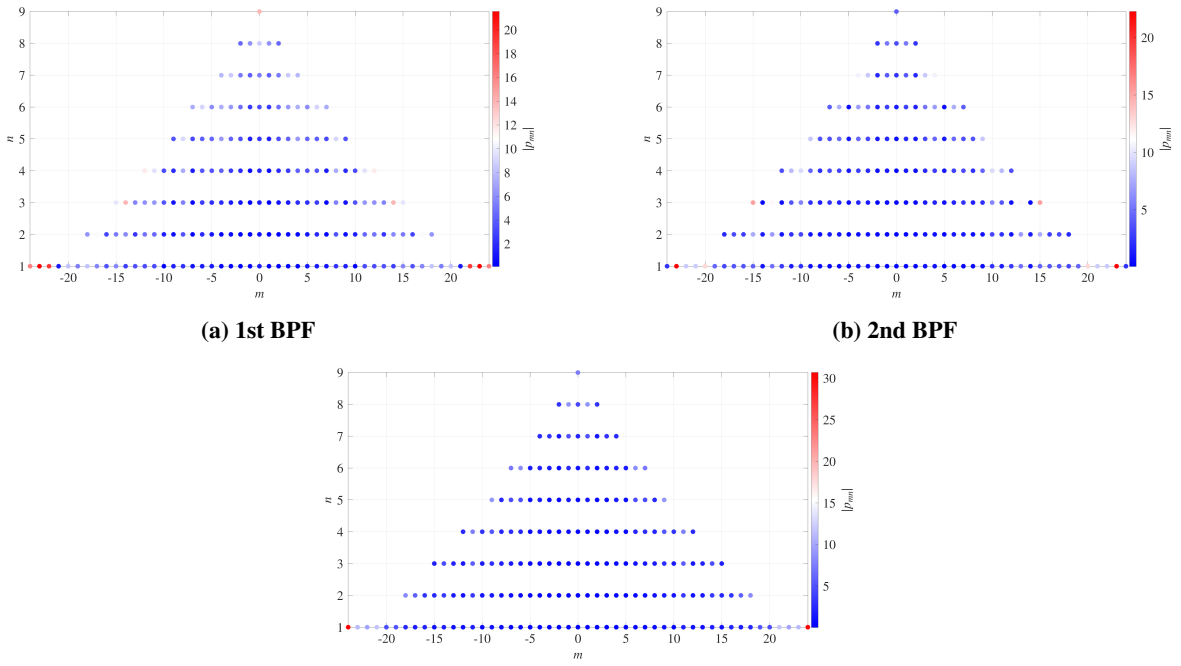

(a) 1st BPF **(b) 2nd BPF**

(c) 3rd BPF

Fig. 9 Modal amplitudes $|p_{mn}|$ at the duct exit $z = 0\,\mathrm{m}$ (the propeller plane) reconstructed by modal decomposition at different BPFs.

Overall, the present results show that the in-duct near-field pressure of a shrouded propeller is not purely acoustic in nature. Instead, it contains both an acoustic like component and a strong additional near-field contribution from the hydrodynamic behaviour. These findings highlight the importance of distinguishing between these components when interpreting in-duct pressure measurements and when assessing how propeller generated sound behaves within the duct. The modal decomposition provides a useful first step towards this separation, although further work is required to improve the robustness of the acoustic filtering procedure, particularly for cut-off modes and for pressure fields close to the propeller plane.

V. Acknowledgments

This work was funded by the UK Department for Science, Innovation and Technology and the Royal Academy of Engineering under the Research Fellowships scheme (RF-2324-23-289).

References

[1] Baddour, B., Joseph, P., McAlpine, A., and Leung, R., "Acoustic radiation characteristics of cutoff modes from ducts," *Journal of Sound and Vibration*, Vol. 541, 2022, p. 117306. https://doi.org/10.1016/j.jsv.2022.117306.

[2] Baddour, B., "Duct effects on acoustic source radiation," Ph.d. thesis, University of Southampton, May 2023.

[3] Baddour, B., Joseph, P., McAlpine, A., and Leung, R., "Duct Effects on Acoustic Source Radiation," *AIAA Journal*, Vol. 62, No. 3, 2024, pp. 1037–1051. https://doi.org/10.2514/1.j063444.

[4] Sha, S., Palleja-Cabre, S., Paruchuri, C., and Joseph, P., "Acoustic Radiation from Finite 'Short' Ducts," *Proceedings of AIAA/CEAS Conference 2026*, AIAA, Brussel, Belgium, 2026.

[5] Guerin, S., "Farfield Radiation of Induct-Cutoff Pressure Waves," *Proceedings of AIAA AVIATION FORUM*, AIAA, Denver, Colorado, 2017. https://doi.org/10.2514/6.2017-4037.

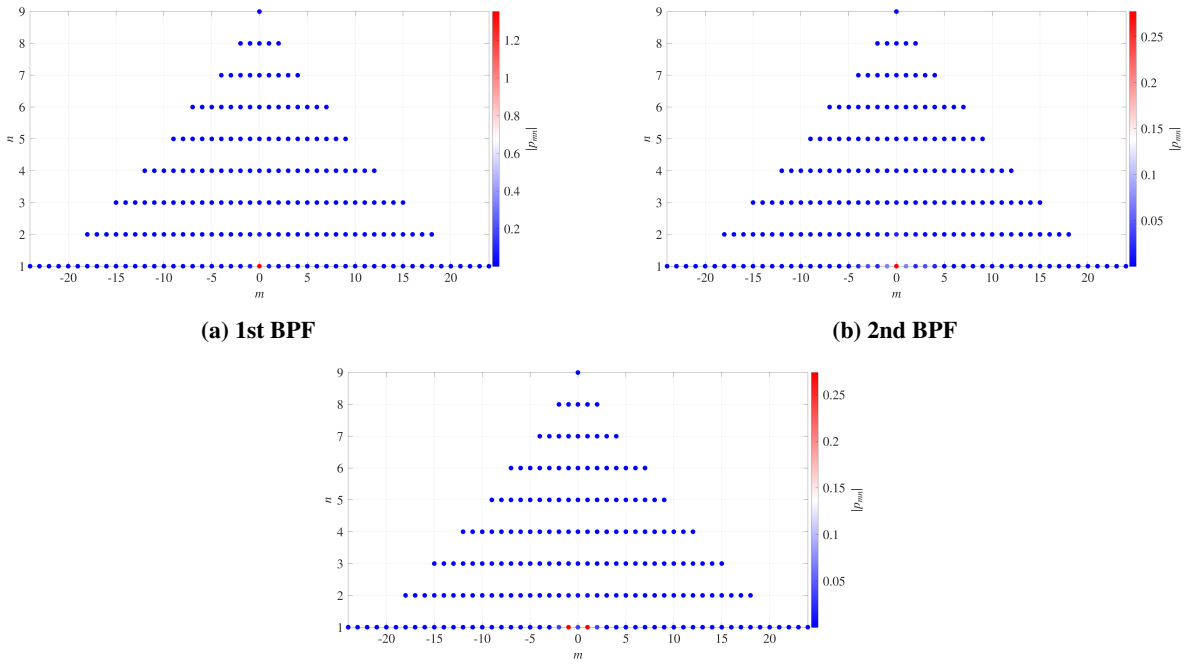

(a) 1st BPF **(b) 2nd BPF**

(c) 3rd BPF

Fig. 10 Modal amplitudes $|p_{mn}|$ at $z = -0.15$ m (duct exit) reconstructed by modal decomposition at different BPFs.

[6] Pereira, A., Finez, A., Leclere, Q., Salze, E., and Souchotte, P., "Modal Identification of a Small-Scale Ducted Fan," *Proceedings of AIAA/CEAS Aeroacoustics Conference 2016*, AIAA, Lyon, France, 2016. https://doi.org/10.2514/6.2016-3063.

[7] Go, S. T., Kingan, M. J., Wu, Y., and Sharma, R. N., "Experimental and numerical investigation of the sound field produced by a shrouded UAV propeller," *Journal of Applied Acoustics*, Vol. 211, 2023. https://doi.org/10.1016/j.apacoust.2023.109523.

[8] Palleja-Cabre, S., Ballgjati, J., Saraceno, I., Joseph, P., Chaitanya, P., and Avallone, F., "Aeroacoustic Investigation of Shrouded Propeller Systems," *Proceedings of AIAA AVIATION FORUM AND ASCEND 2025*, AIAA, Las Vegas, Nevada, 2025. https://doi.org/10.2514/6.2025-3750.

[9] Palleja-Cabre, S., Ballgjati, J., Paruchuri, C., Joseph, P., and Avallone, F., "EXPERIMENTAL INVESTIGATION INTO THE SUPPRESSION OF PROPELLER NOISE USING OVER-TIP-ROTOR LINERS," *Proceedings of Forum Acusticum Euro-Noise 2025*, European Acoustics Association, Malaga, Spain, 2025. https://doi.org/10.61782/fa.2025.0376.

[10] Go, S. T., Kingan, M. J., McKay, R. S., and Sharma, R. N., "Theoretical Investigation of the Turbulent Inflow Noise Produced by a Shrouded Propeller," *28th AIAA/CEAS Aeroacoustics Conference*, American Institute of Aeronautics and Astronautics, Southampton, UK, 2022. https://doi.org/10.2514/6.2022-2831.

[11] Go, S. T., Kingan, M. J., McKay, R. S., and Sharma, R. N., "Turbulent Inflow Noise Produced by a Shrouded Propeller," *Journal of Sound and Vibration*, Vol. 542, 2023, p. 117366. https://doi.org/10.1016/j.jsv.2022.117366.

[12] Go, S. T., Kingan, M. J., Bowen, L., and Azarpeyvand, M., "Noise of a Shrouded Propeller Due to Ingestion of Grid-Generated Turbulence," *Journal of Sound and Vibration*, Vol. 571, 2024, p. 118044. https://doi.org/10.1016/j.jsv.2023.118044.

[13] Cantos, S., Wu, H., Li, X., Zhou, P., and Zhang, X., "Experimental Flow and Aeroacoustic Study of a Ducted Propeller in Axial Flow," *AIAA Journal*, 2026. https://doi.org/10.2514/1.J066347.

[14] Palleja-Cabre, S., Macey, E., Paruchuri, C. C., and Joseph, P., "Reduction of Shrouded Propeller Noise With Over-Tip-Rotor Liners," *30th AIAA/CEAS Aeroacoustics Conference (2024)*, American Institute of Aeronautics and Astronautics, 2024. https://doi.org/10.2514/6.2024-3407.

[15] Avallone, F., Ragni, D., and Casalino, D., "On the effect of the tip-clearance ratio on the aeroacoustics of a diffuser-augmented wind turbine," *Renewable Energy*, Vol. 152, 2020, pp. 1317–1327. https://doi.org/10.1016/j.renene.2020.01.064, URL https://doi.org/10.1016/j.renene.2020.01.064.

[16] Succi, S., *The lattice Boltzmann equation for fluid dynamics and beyond*, 1st ed., Clarendon Press, 2001.

[17] Shan, X., Yuan, X.-F., and Chen, H., "Kinetic theory representation of hydrodynamics: a way beyond the Navier–Stokes equation," *Journal of Fluid Mechanics*, Vol. 550, 2006, pp. 413–441. https://doi.org/10.1017/S0022112005008153.

[18] Chen, S., and Doolen, G., "Lattice Boltzmann method for fluid flows," *Annual Review of Fluid Mechanics*, Vol. 30, 1998, pp. 329–364. https://doi.org/10.1146/annurev.fluid.30.1.329.

[19] Chen, H., Chen, S., and Matthaeus, W., "Recovery of the Navier-Stokes equations using a lattice-gas Boltzmann method," *Physical Review A*, Vol. 45, 1992, pp. R5339–R5342. https://doi.org/10.1103/PhysRevA.45.R5339.

[20] Chen, H., Zhang, R., and Gopalakrishnan, P., "Lattice Boltzmann Collision Operators Enforcing Isotropy and Galilean Invariance," , 8 2015. URL https://patents.google.com/patent/US20150356217A1/en.

[21] Yakhot, V., and Orszag, S., "Renormalization group analysis of turbulence. I. Basic theory," *Journal of Scientific Computing*, Vol. 1, 1986, pp. 3–51. https://doi.org/10.1007/BF01061452.

[22] Teixeira, C., "Incorporating Turbulence Models into the Lattice-Boltzmann Method," *International Journal of Modern Physics C*, Vol. 09, 1998, pp. 1159–1175. https://doi.org/10.1142/S0129183198001060.

[23] Wilcox, D., *Turbulence modelling for CFD (Third Edition)*, DCW Industries, Incorporated, 2006.

[24] Launder, B., and Spalding, D., "The numerical computation of turbulent flows," *Computer Methods in Applied Mechanics and Engineering*, Vol. 3, 1974, pp. 269–289. https://doi.org/10.1016/0045-7825(74)90029-2.

[25] Parry, A. B., "Theoretical Prediction of Counter-Rotating Propeller Noise," Ph.D. thesis, University of Leeds, 1988.